RSC Advances

ROYAL SOCIETY OF CHEMISTRY

www.rsc.org/advances

RSC Advances

ARTICLE

Raman scattering quantitative assessment of the anion composition ratio in Zn(O,S) layers for Cd-free chalcogenide-based solar cells

Received 00th January 20xx,
Accepted 00th January 20xx

DOI: 10.1039/x0xx00000x

www.rsc.org/

M. Guc,[a,†] M. Neuschitzer[a], D. Hariskos,[b] A. Bauer,[b] W. Witte,[b] W. Hempel,[b] L. Calvo-Barrio,[c] P. Pistor,[a] A. Perez-Rodriguez[a,d] and V. Izquierdo-Roca[a]

This work reports the use of Raman scattering for the chemical characterization of Zn(O,S) layers that are being developed as Cd-free alternative for the buffer layer in advanced chalcogenide solar cells. The nanometric thickness of these layers requests the use of resonant excitation conditions, which are strongly sensitive to the alloy composition. In this study Raman spectra were measured with different excitation wavelengths (325 nm, 532 nm) on a set of reference samples with chemical compositions covering the whole range from stoichiometric ZnS to stoichiometric ZnO. The results show the existence of a strong linear dependence of the frequency of the ZnO-like peak on the alloy composition, which provides a simple methodology for the quantitative assessment of the chemical composition in almost all the composition region. In the case of samples with S-rich composition ($0.5 \leq S/(S+O) \leq 1$), the analysis of the relative intensity of the ZnS like peak allows for a complementary assessment of the S/(S+O) content ratio. The characterization of layers grown under conditions similar to those used for the fabrication of chalcogenide solar cells has allowed demonstrating the viability of the proposed methodology for the non-destructive chemical assessment of these advanced buffer layers.

1 Introduction

Chalcogenide thin film solar cells are receiving a strong interest in the last years for the development of cost efficient photovoltaic technologies. This includes chalcopyrite $Cu(In,Ga)(S,Se)_2$ (CIGS) based technologies, that are already at industrial production stage, as well as emerging technologies based in kesterite $Cu_2ZnSn(S,Se)_4$ (CZTS) compounds formed by earth abundant and non-toxic elements. In the first case, CIGS devices have already demonstrated record efficiencies that are higher than those of best polycrystalline Si wafer-based devices, with efficiency values up to 21.7 %. [1] On the other hand, kesterite based devices are still at a research level, and constitute a promising potential alternative to CIGS for mass deployment at terawatt level, where scarcity of In and Ga in the earth crust might be a problem for CIGS. In all these technologies, highest efficiency devices are achieved using a nanometric CdS buffer layer to build a CdS/chalcogenide heterojunction. However, the band gap of CdS is 2.4 eV. It therefore absorbs photons with wavelengths lower than 520 nm, which constitute approximately 24 % of the entire solar spectrum. This parasitic absorption leads to a drop in the external quantum efficiency in the blue-UV spectral region, which limits the photovoltaic conversion efficiency of the solar cells. Replacement of CdS by highly transparent Cd-free alternative buffer layers offers the potential to enhance the device efficiency and is of interest because of the toxicity of Cd, which implies the need for special care of the handling of the Cd-containing waste that is generated during the deposition process. [2]

Among the different alternatives to CdS, Zn(O,S) alloys have been reported as one of the most promising candidates, and high efficiency devices up to 21 % efficiency have already been reported with these layers. [3-7] In this case, control of the O/S content ratio is very important in order to ensure an optimal moderate spike-like conduction band alignment at the absorber/buffer heterojunction. [8] However, the analysis of the anion ratio of these buffer layers by non-destructive techniques is still challenging, being the use of techniques as X-Ray Fluorescence or X-Ray Diffraction compromised by either the presence of interactions between the S and Mo signals (being the back contact in the cells constituted by a Mo thin film) or their very small thickness (typically in the range 20 – 80 nm). Consequently, chemical analysis of the layers typically requires the use of techniques involving sample manipulation

[a] Catalonia Institute for Energy Research (IREC), Jardins de les Dones de Negre 1, 08930 Sant Adrià de Besòs (Barcelona), Spain.
[b] Zentrum für Sonnenenergie- und Wasserstoff-Forschung Baden-Württemberg (ZSW), Stuttgart, Germany.
[c] Centres Científics i Tecnològics CCiTUB, Universitat de Barcelona, C. Lluis Solé i Sabarés 1, 08028 Barcelona, Spain.
[d] IN²UB, Departament d'Electrònica, Universitat de Barcelona, C. Martí i Franquès 1, 08028 Barcelona, Spain.
† Corresponding author. E-mail: mguc@irec.cat

under high vacuum conditions as X-Ray photoelectron spectroscopy (XPS) or Auger electron spectroscopy (AES).

In this context, this work proposes a Raman scattering based methodology for the analysis of the S/(S+O) relative content of the Zn(O,S) buffer layers. Raman scattering is a powerful non-destructive tool very sensitive to both the atomic composition and the crystal quality of the layers, and has already been reported for the quantitative composition analysis of chalcogenide semiconductors, including the assessment of the S/(S+Se) content ratio in sulfo-selenide alloys from the CIGS, CZTS and Zn(S,Se) systems. [9,10,11] Raman scattering analysis of Zn(O,S) solid solutions has already been reported in. [12-15] These previous works showed the existence of a 2-mode behavior characteristic of the solid solution with the observation of two main peaks corresponding to the ZnO-like peak (located at 574 cm^{-1} in ZnO) and the ZnS-like peak (located at 351 cm^{-1} in ZnS). Ref. 15 reported also the existence of a strong bowing of the band gap of the Zn(O,S) solid solution. These authors observed a significant dependence of the frequency of the main ZnO-like Raman peak with the alloy composition. However, this study was limited to the composition region corresponding to O-rich layers ((S/(O+S) ≤ 0.23). In addition, for the used excitation wavelengths (514.5 nm, 488 nm) the penetration depth of scattered photons in these samples is typically higher than 1 micrometer. This compromises the detection of these Raman peaks in the spectra measured from buffer layers, which have a much lower thickness (in the range between 20 – 40 nm), and the spectra are usually dominated by the peaks from the underlying chalcogenide absorber layer in the devices. This implies the need for the use of resonant excitation conditions that allow achieving a strong enhancement of the intensity of the main Raman peaks from the investigated nanometric layers.

In this work, Raman scattering measurements have been performed with different excitation wavelengths (325 nm, 532 nm) using a set of reference samples that were grown with chemical compositions covering the whole range from stoichiometric ZnS to stoichiometric ZnO. UV excitation conditions have been selected as they allow achieving a resonant Raman scattering excitation of the samples with S-rich and O-rich compositions. As previously reported, use of a 325 nm excitation wavelength allows resonant Raman scattering analysis of pure ZnO [16] and ZnS [17] layers, even in the case of samples with nanometric dimensions. On the other hand, for compositions close to S/(S+O) ≈ 0.5, near resonant excitation is achieved using a 532 nm excitation wavelength, due to the strong bowing of the bandgap of the Zn(O,S) system. The analysis of the experimental spectra shows the existence of a clear linear correlation of the frequency of the main ZnO-like mode with the S/(S+O) composition ratio, which provides with a simple methodology for the quantitative assessment of the chemical composition in almost all the composition region. In the case of samples with S-rich composition (0.5 ≤ S/(S+Se) ≤ 1), the analysis of the relative intensity of the ZnS like peak allows for a complementary assessment of the S/(S+Se) content ratio. Finally, the viability of the resonant Raman scattering measurements for the characterization of Zn(O,S) buffer layers has been corroborated using thin layers with thicknesses between 40 nm and 80 nm grown on CIGS and Mo coated substrates.

2 Experimental Details

The Zn(O,S) layers were deposited on Mo coated glass substrates, which were cleaned only prior to the Mo deposition in a Miele glassware-washer for cleanroom laboratories. The deposition was performed by rf magnetron sputtering from different zinc sulfide targets. For all depositions, the sputtering power density was around 1 W/cm^2 and the substrate temperature in the range of 150 °C. The S/(S+O) ratio in the layer was influenced by addition of oxygen into the argon sputtering gas during deposition. The O_2 content in the sputtering gas was successively increased up to 1.7 vol.%, which resulted in Zn(O,S) layers with different compositions down to a S/(S+O) ratio close to pure ZnO. The thicknesses of fabricated layers ranged between 100 and 500 nm. For more details see Table S1 in the supplementary information. The influence of deposition parameters (substrate temperature and O_2 content in sputtering gas) on the composition of reactive sputtered Zn(O,S) layers as used in this work is reported by Eicke et al. [18]

The samples have been characterized by X-Ray Diffraction (XRD) and X-Ray Photoelectron Spectroscopy (XPS) techniques, in addition to Raman scattering. XRD has been reported as a suitable technique for the chemical analysis of the S/(S+O) content ratio in Zn(O,S) solid solutions grown on glass and sapphire substrates with hexagonal crystal structure. [19] In this case, the position of the 002 peak shows a linear dependence with the S/(S+O) content ratio, in agreement with the Vegard's law. XRD measurements were made in $\theta/2\theta$ configuration using a Bruker D8 diffractometer with copper K_α radiation. Figure S1 from the supplementary information shows the diffractograms measured on the different samples. In the diffractograms measured from samples close to pure ZnO the presence of the 002 and 100 peaks indicate a hexagonal crystal structure of the films. [20] However, for samples close to pure ZnS, these peaks from the hexagonal structure are missing, and only one peak is observed which has been assigned to the 111 peak of the cubic structure. [21] As a result, a phase transition from hexagonal to cubic is expected within the mixing range. In addition, the diffractograms from samples with S/(S+O) close to 0.5 show a very broad band with very low intensity, in agreement with the worsening of the crystalline quality that has also been observed by Raman (as described in the next section). This agrees with the behavior reported in Ref. 21 for Zn(O,S) layers that were grown on quartz and Mo coated glass substrates, where the XRD peaks roughly follow Vegard's law. These features compromise the use of the XRD measurements for the analysis of the S/(S+O) content ratio of the layers.

XPS experiments were performed in a PHI 5500 Multitechnique System (from Physical Electronics) with a monochromatic X-ray source (Aluminium Kα line of 1486.6 eV energy and 350 W), placed perpendicular to the analyzer axis and calibrated using the $3d_{5/2}$ line of Ag with a full width at half maximum (FWHM) of 0.8 eV. The analyzed area was a circle of

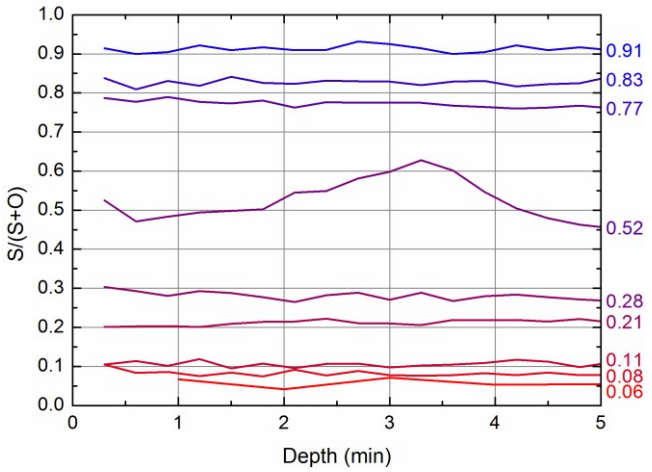

Fig. 1: Depth resolved XPS S/(S+O) ratio profile of analyzed Zn(O,S) solid solutions measured on the 100 nm surface region from the different samples. Numbers on the right correspond to the average composition measured at this surface region.

0.8 mm diameter, and the selected resolution for survey spectra was 187.5 eV of pass energy and 0.8 eV/step, while for the spectra of the different elements was 23.5 eV of pass energy and 0.1 eV/step. All measurements were made in an ultra-high vacuum (UHV) chamber pressure at about 5×10^{-9} torr, and the first 100 nm surface region of the samples was sputtered with an Ar^+ beam (4 keV source energy) with a 20 nm/min sputter rate. In order to correct the binding energy axis for all the samples the single peak that appears in the $Cu2p_{3/2}$ region has been fixed at 932.0 eV. This has been proved to do the same results that placing the contribution of the adventitious carbon from the C1s peak present in the surface measurements at 284.8 eV. The raw XPS spectra measured on a representative sample are plotted in figure S2 from the supplementary information. Figure 1 shows the depth resolved S/(S+O) ratio profiles measured in the 100 nm thick surface region from the different samples. As can be seen only in case of the sample close to S/(S+O) ≈ 0.5 it was found some deviation through the thickness. This suggests the existence of an inhomogeneous sputtering growth of the samples with compositions close to this point. For all the other samples, the performed measurements show a constant depth resolved composition.

The Raman spectra were excited with a He-Cd laser (325 nm wavelength line) and a frequency doubled YAG:Nd solid-state laser (532 nm) and recorded using a *i*HR320 Horiba Jobin Yvon spectrometer in conjunction with a CCD detector. The measurements were performed in backscattering configuration through an Olympus objective. Excitation power density on the sample surface was ~ 0.1 kW/cm^2 for UV and ~ 1.5 kW/cm^2 for green lasers, which allowed avoiding the presence of thermal effects in the spectra (this implied the need to perform a previous analysis of spectra measured with different excitation powers on the different samples and for the different excitation wavelengths). Penetration depth in the Zn(O,S) samples depends on their composition, and ranges between < 100 nm for the UV excitation line and about 1 µm for the 532 nm excitation wavelength for the samples with composition close to the ZnS and ZnO parent semiconductors.

The applicability of the proposed method to assess the anion ratio in Zn(O,S) solid solutions has also been checked using thin films that were grown by chemical bath deposition (CBD) using the same process conditions than those reported for the growth of the buffer layers in advanced chalcogenide cells, using a bath mixture of $ZnSO_4$, NH_4OH and thioacetamide in the presence of a chelating agent at 80°C. [22] The variation of the S/(S+O) ratio in the CBD Zn(O,S) layers was performed by varying the pH value between 10 – 12 as well as the ratio of chelating ligand to ammonia concentration. After CBD, the Zn(O,S) layers were not annealed. The films were grown with thicknesses between 40 nm and 80 nm either on Mo coated soda lime glass (SLG) and on CIGS absorber layers.

3 Raman spectra from Zn(O,S) samples

The room temperature stable structures of ZnO and ZnS compounds are the wurtzite (WZ) and zinc-blended (ZB) structures, respectively. [23-25] However, at higher temperatures both of these compounds have also the cross polymorphs, ZnO in ZB structure and ZnS in WZ structure. WZ structure can be characterized by four atoms in the elemental cell from an hexagonal Bravais lattice with space group $P6_3mc$, [23] while the ZB structure has only two atoms in the elemental cell with a cubic Bravais lattice and space group $F\bar{4}3m$. [24,25] According to group theory analysis, $A_1 \oplus E_1 \oplus 2E_2$ modes are Raman active for WZ and only T_2 mode is Raman active for ZB. From these modes, only the E_2 one is not polar, while A_1, E_1 and T_2 modes exhibit the TO/LO splitting. [24,25]

This work is centered in the analysis of the main ZnO-like and ZnS-like Raman peaks in the spectra. In the case of ZnS, the main Raman peak is located at 351 cm^{-1}, independently of the crystalline structure. [24,25] In the case of the WZ structure this peak is assigned to a sum of A_1(LO) and E_1(LO) vibrational modes, while in case of the ZB structure it is assigned to the T_2(LO) mode. In the case of WZ ZnO, the main peak at 574 cm^{-1} is assigned to the A_1(LO) mode. Thus for convenience we simplified the notation of the ZnS-like and ZnO-like peaks in the Zn(O,S) compound with LO_{ZnS} and LO_{ZnO}, respectively.

Figure 2 shows the Raman spectra measured from the different samples using the UV excitation wavelength (the spectra measured with 532 nm excitation wavelength show a similar behavior and are plotted in Figure S3 from the supplementary information). The spectra measured from the Zn(O,S) samples show the double mode behavior of the LO mode, being these peaks the dominant ones in all the spectra. From these spectra it is clear that the ZnS-like LO peak maintains its position at around 350 cm^{-1} for the whole set of samples, while the ZnO-like LO peak shows a significant shift (of up to more than 150 cm^{-1}) towards lower frequencies when the S content in the layers increases. This can be explained by the significant difference in the S and O molar masses. Thus the vibrations of the lighter O atoms are more sensitive to the

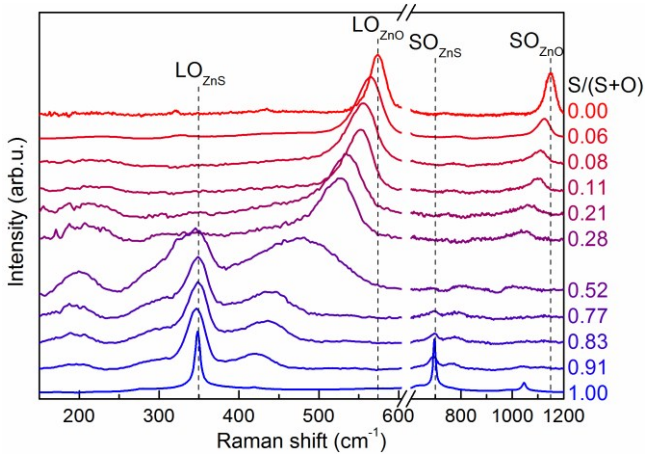

Fig. 2: Raman spectra of Zn(O,S) solid solutions excited by 325 nm laser line, normalized to the intensity of the most intense peak (LO_{ZnO} for samples with S/(S+O) < 0.5, LO_{ZnS} for samples with S/(S+O) > 0.5). The spectra of ZnO and ZnS thin films are added for reference. Numbers on the right correspond to the average composition measured at the 100 nm surface region from the different samples.

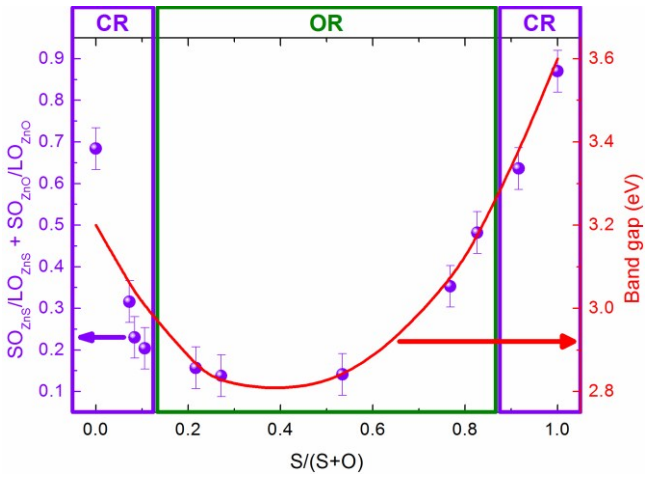

Fig. 3: Sum of relative intensity of second order (SO) Raman peaks in relation to the corresponding first order ones measured with 325 nm excitation wavelength (dots) and band gap bowing (solid line) in Zn(O,S) alloys versus S/(S+O) composition ratio measured by XPS. CR and OR ranges are close to and out of resonant conditions, respectively.

presence of S atoms in the lattice, while the vibrations of the heavier S atoms are almost not affected by the presence of the lighter O atoms in the lattice.

The spectra are also characterized by the second order peaks corresponding to both LO_{ZnO} and LO_{ZnS} modes (labelled as SO_{ZnO} and SO_{ZnS} in the figure). The intensity of these peaks is higher for the samples with compositions close to the parent ZnS and ZnO compounds, and decreases as the S/(S+O) content ratio tends to S/(S+O) ≈ 0.5. This behavior agrees with the bowing of the band gap of the alloy, [15] which determines a decrease of the resonant excitation conditions achieved with the UV excitation wavelength when the composition of the alloy goes away from the S- and O-rich composition regions. This behavior is clearly shown in Figure 3, where the sum of relative intensities of the SO_{ZnO} and SO_{ZnS} peaks in relation to the corresponding first order ones is plot together the band gap bowing (according to the equation proposed in Ref. 15) versus the S/(S+O) content ratio measured in the surface region of the samples. The correlation between the experimental points and the bandgap bowing corroborates the gradual loss of resonance excitation conditions when using the 325 nm excitation wavelength as the composition of the samples tends to S/(S+O) ≈ 0.5. This is also accompanied by a significant increase of the full width at the half maximum (FWHM) of both LO peaks. This is likely related to the influence of structural disorder yielding to a worsening of the crystalline quality of the layers that is induced by the partial substitution of S by O atoms in the ZnS lattice.

Additionally to the intense LO modes the Raman spectra show a clear band at the 160 – 230 cm^{-1} spectral region, which relative intensity is maximal in the case of the sample with composition close to S/(S+O) = 0.5. This band is likely related to overtones of transversal acoustic modes out of the Γ point of the Brillouin zone and/or activation of some others non-center Raman inactive modes. [26] This agrees with the worsening of the crystalline quality observed by the increase of the FWHM of the main Raman peaks as the S/(S+O) ratio tends to 0.5.

4 Correlation with S/(S+O) relative content in the alloy

Figure 4 shows the plot of the frequency of the LO_{ZnO} peak from the spectra in Figure 2 versus the S/(S+O) content ratio of the samples. These data are characterized by the existence of a very linear behavior for almost all the range of compositions analyzed (from stoichiometric ZnO up to S-rich Zn(O,S) layers with S/(S+O) content ratio higher than 0.9).

The solid line in the figure corresponds to the fitting of these data with the linear equation:

$$\omega[cm^{-1}] = 574.0 - 170.8\left(\frac{S}{S+O}\right). \quad (1)$$

Here the values of S and O content are in at. %. The strong linearity of the experimental data is reflected in the very high value achieved for the R2 fitting factor, R2 = 0.99996. This gives a strong validity for the simple empirical equation that is proposed for the quantitative estimation of the S/(S+O) content ratio in the analyzed layers. As shown in Figures 2 and 4, even in the case of samples with composition S/(S+O) = 0.91, the resonance achieved with the UV excitation wavelength allows detection of the ZnO-like peak with enough sensitivity to be used for the composition assessment.

For samples with compositions corresponding to S/(S+O) > 0.5, a complementary assessment of the sample composition can be achieved from the analysis of the relative integral intensity of the LO_{ZnS} peak in relation to the sum of intensities of the LO_{ZnS} and LO_{ZnO} peaks. Figure 5 shows the plot of these data versus the S/(S+O) content ratio from the analysis of the

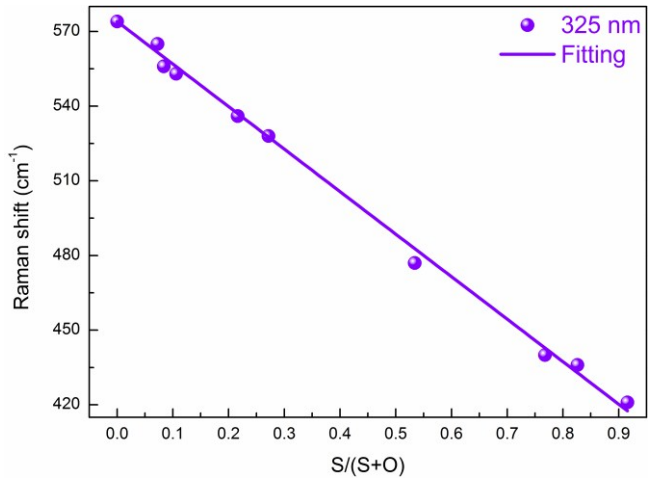

Fig. 4: Frequency of ZnO-like LO peak measured with 325 nm excitation wavelength versus S/(S+O) ratio measured by XPS in the surface region from the Zn(O,S) solid solutions. The solid line represents the linear fit to the experimental data.

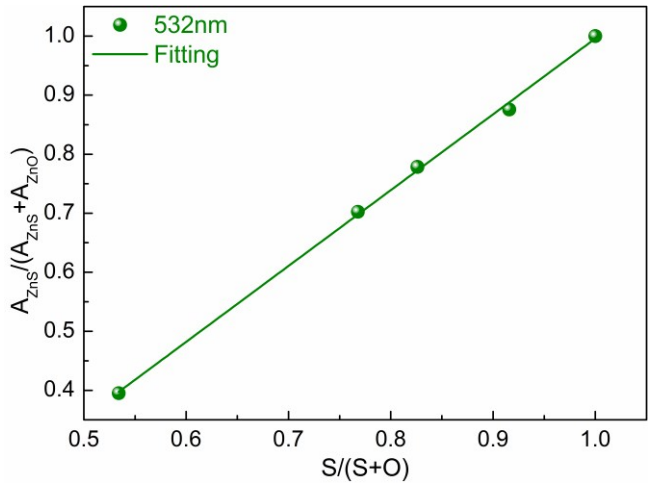

Fig. 5: Relative integral intensity of LO_{ZnS} peak in relation to the sum of intensities of the LO_{ZnS} and LO_{ZnO} peaks measured with 532 nm excitation wavelength, versus S/(S+O) content ratio measured by XPS in the surface region of the samples, for samples with S/(S+O) > 0.5. The solid line is the linear fitting of the experimental points.

Raman spectra measured with 532 nm excitation wavelengths that are plotted in Figure S3 in the supplementary information. In this analysis the spectral region defined for the calculation of the integral intensity of the LO_{ZnS} peak has been fixed at 315 – 380 cm^{-1}, while for the LO_{ZnO} peak a spectral range was used equal to the FWHM of the peak and centered on the peak maximum. The later allowed to minimize the influence of the strong LO_{ZnO} peak shift and broadening from sample to sample. As shown in Figure 5, the relative intensity data measured with 532 nm excitation wavelength show a clear linear behavior with the relative S/(S+O) content ratio. The solid green line in the figure shows the linear fitting of these data according to the simple equation:

$$\frac{A_{ZnS}}{A_{ZnS}+A_{ZnO}} = -0.15 + 1.15\left(\frac{S}{S+O}\right), \quad (2)$$

with fitting factor R2 = 0.997. This contrast with data measured under UV excitation (not shown here), where the data cannot be fitted with a simple linear behavior. These differences could be related to the strong dependence of the intensity of the peaks from the spectra measured with different excitation wavelengths on the existence of resonant excitation conditions. As has been already indicated, the Zn(O,S) system is characterized by the existence of a strong bowing of the bandgap and this determines a decrease of the band gap down to a value of 2.5 eV for an alloy composition of S/(S+O) = 0.5. [15] This means that the two used laser lines have a different behavior in the S/(S+O) composition region from 0.5 to 1.0: For the 532 nm excitation wavelength, resonant excitation conditions are nearly achieved for compositions close to S/(S+O) = 0.5 and these conditions are gradually lost as the S content increases. In contrast to this, under UV excitation the spectra measured form samples with compositions close to S/(S+O) = 0.5 are out of resonance, and they become resonant as the S content increases. For the samples with S/(S+O) content ratio lower than S/(S+O) = 0.5, the strong decrease observed in the intensity of the ZnS-like peak (with values lower than the noise level in the spectra from samples with S/(S+O) < 0.28) does not allow for the analysis of these data.

5 Application to Zn(O,S) nanometric buffer layers

Figure 6 shows the Raman spectra measured with the 325 nm excitation wavelength on the Zn(O,S) layers that were grown on Mo-coated SLG substrates and CIGS absorber layers with thicknesses between 40 and 80 nm. As already indicated, these correspond to the conditions used for the fabrication of

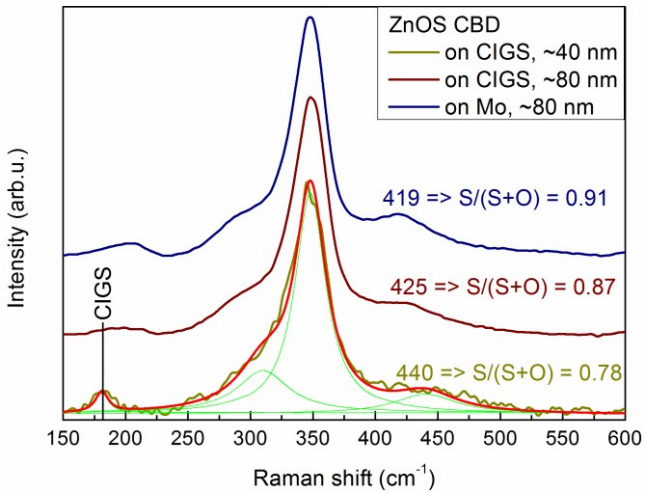

Fig. 6: Raman spectra (normalized to the intensity of the main peak) excited by 325 nm laser line in Zn(O,S) thin films made by CBD on different substrates. The numbers indicate the frequency of the ZnO-like LO peak position and the corresponding values of the S/(S+O) ratio estimated according to the linear equation given in the previous section. The bottom spectrum (dark yellow line) was fitted (red curve) with Lorentzian curves (green lines).

high efficiency CIGS solar cells. [22] The Raman spectra show the shape characteristic of that corresponding to S-rich Zn(O,S) alloys, with the presence of a dominant LO_{ZnS} peak. Measurements performed with the 532 nm excitation wavelength have not allowed to detect the peaks characteristic of the Zn(O,S) alloy, in agreement with the lack of resonance expected for samples with S-rich composition at this excitation wavelength.

In these spectra, the S/(S+O) content ratio has been estimated from the frequency of the LO_{ZnO} peak, according to the linear relationship that was given in the previous section. This gives values of the S/(S+O) content ratio between 0.78 and 0.91 for the different layers. For the thinnest layer (with a thickness of 40 nm), the spectrum also shows the Raman peak from the underlying CIGS absorber layer. Due to the low intensity of the Zn(O,S) Raman peaks, a fitting of the Raman spectra was required here for the determination of the frequency of the LO_{ZnO} peak. The fit has been performed using Lorentzian curves for the different modes. The uncertainty in the determination of the frequency of the LO_{ZnO} peak is of the order of 5 cm^{-1}, which determines an uncertainty in the determination of the S/(S+O) content ratio of ± 0.04. These data corroborate the viability of the proposed methodology for the non-destructive composition assessment of Zn(O,S) buffer layers used in these PV technologies, in spite of their nanometric thickness.

Conclusions

Raman scattering measurements performed under resonant excitation conditions have been demonstrated for the non-destructive assessment of the composition of Zn(O,S) nanometric buffer layers that are being developed for advanced Cd-free chalcogenide solar cells. Calibration of the dependence of the frequency of the LO_{ZnO} peak and of the relative integral intensity of the LO_{ZnS} peak with the alloy composition gives simple linear relationships that can be used for the whole range of alloy compositions, from stoichiometric ZnO up to stoichiometric ZnS. The detailed analysis of these spectra corroborates the existence of a strong dependence of the resonance excitation conditions on the alloy composition, that is related to the strong bowing of the band gap of the Zn(O,S) system. The analysis also shows existence of a significant worsening in the crystalline quality of the layers grown with compositions close to S/(S+O) = 0.5, which is likely due to chemical disorder effects related to the presence of a random distribution of S and O atoms in the Zn(O,S) lattice of the solid solution.

Acknowledgements

This research was supported by the NovaZOlar project from the SOLAR-ERA.NET International program (subproject ref. PCIN-2013-193 funded by Spanish MINECO), by the MINECO (Ministerio de Economía y Competitividad de España) under the SUNBEAM project (ENE2013-49136-C4-1-R) and by European Regional Development Founds (ERDF, FEDER Programa Competitivitat de Catalunya 2007–2013). Authors from IREC and the University of Barcelona belong to the M-2E (Electronic Materials for Energy) Consolidated Research Group and the XaRMAE Network of Excellence on Materials for Energy of the "Generalitat de Catalunya". P.P. is grateful to the EC for funding under grant agreement No. 625840 ("JumpKEST"). Authors from ZSW are grateful to the projects NovaZOlar (contract 0325749A) and CIS-ProTec (contract 0325715), both financed by the Federal Ministry for Economic Affairs and Energy.

References

1. P. Jackson, D. Hariskos, R. Wuerz, O. Kiowski, A. Bauer, T. M. Friedlmeier and M. Powalla, *Phys. Status Solidi RRL*, 2015, **9**, 28.
2. K. Xerxes Steirer, Rebekah L. Garris, Jian V. Li, Michael J. Dzara, Paul F. Ndione, Kannan Ramanathan, Ingrid Repins, Glenn Teetera, Craig L. Perkins, *Phys. Chem. Chem. Phys.*, 2015, **17**, 15355.
3. T. M. Friedlmeier, P. Jackson, A. Bauer, D. Hariskos, O. Kiowski, R. Wuerz and M. Powalla, *IEEE Journal of Photovoltaics*, 2015, **5**, 1487.
4. M. Bär, A. Ennaoui, J. Klaer, T. Kropp, R. Sáez-Araoz, N. Allsop, I. Lauermann, H.-W. Schock and M. C. Lux-Steiner, *J. Appl. Phys.*, 2006, **99**, 123503.
5. N. Naghavi, D. Abou-Ras, N. Allsop, N. Barreau, S. Bucheler, A. Ennaoui, C.-H. Fischer, C. Guillen, D. Hariskos, J. Herrero, R. Klenk, K. Kushiya, D. Lincot, R. Menner, T. Nakada, C. Platzer-Bjorkman, S. Spiering, A. N. Tiwari and T. Torndahl, *Prog. Photovolt: Res. Appl.*, 2010, **18**, 411.
6. Reiner Klenk, Alexander Steigert, Thorsten Rissom, Dieter Greiner, Christian A. Kaufmann, Thomas Unold and Martha Ch. Lux-Steiner, *Prog. Photovolt: Res. Appl.*, 2014, **22**, 161.
7. Markus Neuschitzer, Karla Lienau, Maxim Guc, Lorenzo Calvo Barrio, Stefan Haass, Jose Marquez Prieto, Yudania Sánchez, Yaroslav Romanyuk, Alejandro Pérez-Rodríguez, Victor Izquierdo-Roca and Edgardo Saucedo, *J. Phys. D: Appl. Phys.* (in-print).
8. T. Adler, M. Botros, W. Witte, D. Hariskos, R. Menner, M. Powalla and A. Klein, *Phys. Status Solidi A,* 2014, **211**, 1972.
9. C. Insignares-Cuello, F. Oliva, M. Neuschitzer, X. Fontané, C. Broussillou, T. Goislard de Monsabert, E. Saucedo, C.M. Ruiz, A. Pérez-Rodríguez and V. Izquierdo-Roca, *Sol. Energy Mater. Sol. Cells*, 2015, **143**, 212.
10. Mirjana Dimitrievska, Galina Gurieva, Haibing Xie, Alex Carrete, Andreu Cabot, Edgardo Saucedo, Alejandro Pérez-Rodríguez, Susan Schorr and Victor Izquierdo-Roca, *J. Alloys Compd.* 2015, **628**, 464.
11. M. Dimitrievska, H. Xie, A. J. Jackson, X. Fontané, M. Espíndola-Rodríguez, E. Saucedo, A. Pérez-Rodríguez, A. Walsh and V. Izquierdo-Roca, *Phys. Chem. Chem. Phys.*, 2015, DOI: 10.1039/C5CP04498G.
12. Yunbin He, Liangheng Wang, Lei Zhang, Mingkai Li, Xunzhong Shang, Yanyan Fang and Changqing Chen, *J. Alloys Compd.,* 2012, **534**, 81.
13. Yunbin He, Lei Zhang, Liangheng Wang, Mingkai Li, Xunzhong Shang, Xiong Liu, Yinmei Lu and Bruno K. Meyer, *J. Alloys Compd.*, 2014, **587**, 369.
14. Bruno K. Meyer, Angelika Polity, Baker Farangis, Yunbin He, Dietmar Hasselkamp, Thorsten Krämer, Changzhong Wang, Ute Haboeck and Axel Hoffmann, *Phys. Stat. Sol. (c)*, 2004, **1**, 694.
15. Angelika Polity, Bruno K. Meyer, Thorsten Krämer, Changzhong Wang, Ute Haboeck and Axel Hoffmann, *Phys. Stat. Sol. (a)*, 2006, **203**, 2867.

16. Cristina Insignares-Cuello, Xavier Fontané, Yudania Sánchez-González, Marcel Placidi, Cedric Broussillou, Juan López-García, Edgardo Saucedo, Verónica Bermúdez, Alejandro Pérez-Rodríguez and Victor Izquierdo-Roca, *Phys. Status Solidi (a)*, 2015, **212**, 56.
17. Andrew Fairbrother, Victor Izquierdo-Roca, Xavier Fontané, Maria Ibáñez, Andreu Cabot, Edgardo Saucedo and Alejandro Pérez-Rodríguez, *CrystEngComm*, 2014, **16**, 4120.
18. A. Eicke, T. Ciba, D. Hariskos, R. Menner, C. Tschamber and W. Witte, Depth profiling with SNMS and SIMS of Zn(O,S) buffer layers for Cu(In,Ga)Se_2 thin-film solar cells, Surf. Interface Anal. 45, 1811–1820 (2013)
19. M. Jaquez, K.M. Yu, M. Ting, M. Hettick, J.F. Sanchez-Royo, M. Wełna, A. Javey, O.D. Dubon, W. Walukiewicz, *J. Appl. Phys.*, 2015, **118**, 215702.
20. A. Grimm, D. Kieven, I. Lauermann, M.Ch. Lux-Steiner, F. Hergert, R. Schwieger, R. Klenk, *EPJ Photovolt.*, 2012, **3**, 30302.
21. A. Grimm, D. Kieven, R. Klenk, I. Lauermann, A. Neisser, T. Niesen, J. Palm, *Thin Solid Films*, 2011, **520**, 1330.
22. D. Hariskos, R. Menner, P. Jackson, S. Paetel, W. Witte, W. Wischmann, M. Powalla, L. Bürkert, T. Kolb, M. Oertel, B Dimmler and B. Fuchs, *Prog. Photovolt: Res. Appl*., 2012, **20**, 534.
23. Hadis Morkoc and Umit Ozgur, *Zinc Oxide: Fundamentals, Materials and Device Technology*, WILEY-VCH Verlag GmbH & Co. KGaA, Weinheim, 2009.
24. Y. C. Cheng, C. Q. Jin, F. Gao, X. L. Wu, W. Zhong, S. H. Li and Paul K. Chu, *J. Appl. Phys.*, 2009, **106**, 123505.
25. O. Brafman and S. S. Mitra, *Phys. Rev.*, 1968, **171**, 931.
26. Ramon Cuscó, Esther Alarcón-Lladó, Jordi Ibáñez, Luis Artús, Juan Jiménez, Buguo Wang and Michael J. Callahan, *Phys. Rev. B*, 2007, **75**, 165202.